Journal of Electrochemical Science and Technology
Vol. 3, No. 4, 2012, 178-184
http://dx.doi.org/10.5229/JECST.2012.3.4.178

Journal of Electrochemical Science and Technology

Electrodeposited Nano-flakes of Manganese Oxide on Macro-porous Ni Electrode Exhibiting High Pseudocapacitance

F. Gobal and S. Jafarzadeh†
Department of Chemistry, Sharif University of Technology, P.O. Box 11365-9516, Tehran, Iran

ABSTRACT :

A porous nickel (P-Ni) substrate was prepared by selective leaching of zinc from pressed pellets containing powders of Ni & Zn in 4 M NaOH solution. Anodic deposition of manganese oxide onto the porous Ni substrate (MnO_x/P-Ni) formed nano-flakes of manganese oxide layers as revealed in SEM studies. Pseudocapacitance of this oxide electrode was evaluated by cyclic voltammetry (CV) and chronopotentiometry (CHP) in 2 M NaOH solution. The specific capacitance of the Mn oxide electrode was as high as 1515 F g^{-1}, which was ten times higher than Mn oxide deposited on a flat Ni-ribbon. 80% of capacity was retained after 200 charge/discharge cycles. The system showed no loss of activity in dry form over period of days. The impedance studies indicated highly conducting MnO_x/P-Ni substance and the obtained specific capacitance from impedance data showed good agreement with the charge/discharge measurements.

Keywords : Mn oxide, Nano-flakes, Porous Ni substrate, Supercapacitor

(Received December 20, 2012 : Accepted December 30, 2012)

1. Introduction

Electrochemical supercapacitors are the charge-storage devices that have larger power density and longer cycle life compared to batteries and higher energy density compared to conventional capacitors.[1] The natural abundance and low cost of Mn oxide, accompanied by its satisfactory electrochemical performance in aqueous electrolytes and environ- mental compatibility, have made it one of the most promising electrode materials for supercapacitors. Owing to the fast, continuous, and reversible redox reaction of Mn oxide, pseudocapacitive behavior of Mn oxide electrode can be realized.[2-4] Since the capacitance of Mn oxide is associated with the reversible faradaic reaction between its trivalent and tetravalent states,[3-5] the theoretical specific capacitance of MnO_2 should be around 1380 F g^{-1}.[4] However, both poor electronic and ionic conductivity of Mn oxide prevent approaching the ideal electrochemical performance.[6,7] The typical specific capacitances of Mn oxides reported in the literature are in the range of 100-250 F g^{-1} [2,6-12] except for the extremely thin oxide films[3,4] where higher capacitance have been realized. In order to promote the utilization and reactivity of Mn oxide and further improve its pseudocapacitive performance, two methods have been adopted. (i) Using anodized aluminum oxide (AAO) templates to prepare Mn oxide nanowire arrays.[13-15] The resulting ordered Mn oxide having high surface area was found to have a specific capacitance of 254 F g^{-1}, as reported by Xu *et al*.[15] (ii) Using carbon nanotubes (CNTs) to fabricate Mn oxide/CNTs composite electrodes.[16-19] Mn oxide was highly dispersed onto CNTs which provides electronic conductivity paths and a network of open mesopores. According to the data reported by Lee *et al*.,[19] specific capacitance as high as 415 F g^{-1} have been achieved. However, both processes involving AAO and CNTs are too complicated and expensive to be used in practi-

†Corresponding author. Tel.: +98-21-6005718
E-mail address: jafarzadeh@mehr.sharif.ir

cal applications. On the other hand, a nanoporous Ni electrode prepared by a simple selective electrochemical de-alloying process of Ni_xCu_{1-x} alloy was demonstrated as a new generation of nanoporous electrodes with enhanced coercivity and magnetic anisotropy.[20)]

The purpose of the present work is to prepare dispersed Mn oxide onto a highly porous Ni substrate by a simple electrochemical method and to investigate its usefulness as electrode material for use in electrochemical capacitors.

2. Experimental

Nickel and zinc powders, manganese sulphate, and NaOH used in this work were analytical grade Merck products and water was de-ionized. Equal amounts of Ni and Zn (particle size was 63 μm) were thoroughly mixed and pressed at 8 t cm^{-2}. The prepared pellets were leached in 4 M NaOH for 48 h to remove zinc. Consequently, a porous Ni (P-Ni) pellet was obtained. It was placed in distilled water for 2 h to remove NaOH from porosities. The electrochemical cell used in this study was a conventional three electrode cell with the porous Ni pellet forming the working electrode, a Pt ribbon was the auxiliary electrode and a saturated calomel electrode (SCE) was used as the reference electrode. All potentials are reported against SCE. All electrochemical depositions studies, and capacitance measurements were performed by Behpajoo 2063 + galvanostat/potentiostat. 2 M NaOH solution was used in electrochemical studies. Chemical compositions were determined by energy dispersive spectroscopy (EDS) in a scanning electron microscope (VEGA\\ Tescan).

Mn oxide was anodically deposited onto the prepared porous Ni substrate from 1 M $MnSO_4$ aqueous solution to form MnO_x/P-Ni. An anodic potential of 1 V/SCE was applied for 900 *s* to deposit Mn oxide according to the following reaction:[27)]

$$Mn^{2+} + 2H_2O \rightarrow MnO_2 + 4H^+ + 4e \quad (1)$$

The weight of deposited Mn oxide on 1 cm^2 geometric area of Ni-pellet was 1.1×10^{-3} g. The electrodeposited films were washed in running distilled water and dried at room temperature. The same amount of Mn oxide was also deposited on a Ni ribbon and used as a reference. Electrochemical performances of the two electrodes were evaluated by cyclic voltammetry (CV), charge/discharge and chronopotentiometry (CP) studies in 2 M NaOH at 25°C. Cycles stability of the electrodes was investigated in the two courses of 100 charge/discharge cycles.

3. Results and Discussion

Elemental analysis was performed by energy dispersive spectroscopy (EDS) and the results for MnO_x/P-Ni sample are presented in Fig. 1. Peaks due to Mn, Ni and oxygen were observed in the spectrum with the weight ratio of 27.78:22.49:46.05 (Mn:Ni:O), which confirms the presence of Mn oxide and Ni in this pellet.

Fig. 2(a) and (b) present the SEM's of Mn oxide/P-Ni at both low and high magnifications. At low magnification macropores formed due to the leaching of Zn

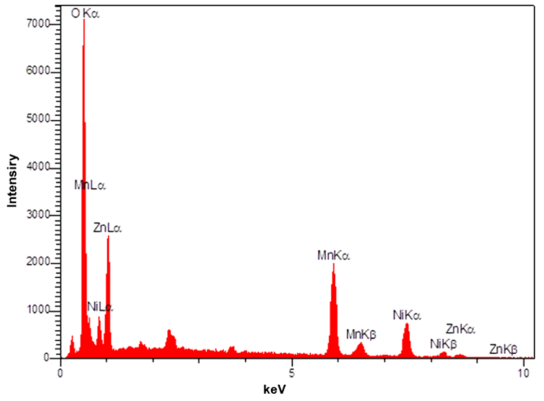

Fig. 1. The EDS of MnO_x/P-Ni.

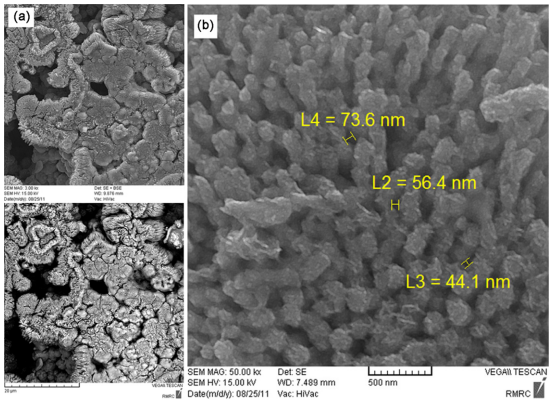

Fig. 2. The SEM of MnO_x/P-Ni at magnification of (a) 3000x, (b) 50000x.

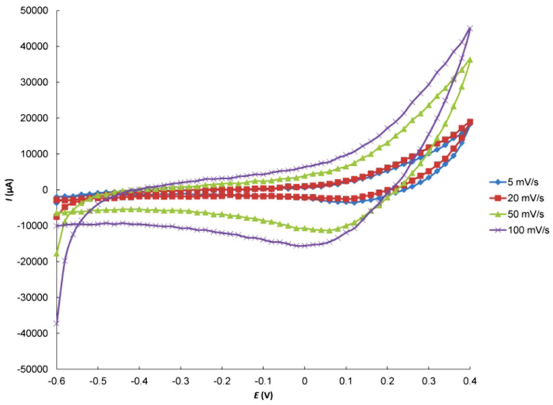

Fig. 3. CVs of porous Ni in 2 M NaOH electrolyte at different scan rates.

can be seen. In the pore mouths flakes (blades) of Mn oxide have been deposited. Looking sideway inside the pores at higher magnification, Fig. 2(b), clearly shows the flakes (blades) of Mn oxide that have fairly uniform structure/size and forming mesopores. The thickness of the flakes is in the nano-scale range and it is likely that most of the material can indeed undergo redox processes that give rise to high capacitance. Interestingly little or no Mn oxide has formed on the flat surface of Ni pellets. Some Ni oxide appearing as white spots or spirals are on the surface but virtually all Mn oxide flakes are formed at the macropores mouths.

Fig. 3 shows cyclic voltammograms for porous Ni substrate in the 2 M NaOH electrolyte.

It is noted that the Ni slightly dissolves and oxidized as the potential is swept beyond 0.2 V/ SCE in alkaline electrolyte to form NiOOH:

$$Ni(OH)_2 + OH^- \rightarrow NiOOH + H_2O + e^- \quad (2)$$

Due to high areas large current is drawn and the sweep is terminated at 0.4 V/SCE. The reduction peak is observed in the cathodic sweep.

The average capacitance (C) of porous Ni pellet is calculated using:

$$C = \frac{I}{\frac{dV}{dt}} \quad (3)$$

Where (I) is the mean current along the voltammogram and is the potential sweep rate.[6)]

The specific capacitance (F g^{-1}) of porous Ni electrode is obtained through dividing C by its respective weight.

The specific capacitance decreased from 96 F g^{-1} to 20 F g^{-1} as the potential scan rate was increased from 5 to 100 mV s^{-1}. The decrease in capacitance with the scan rate is attributed to the presence of active sites deep inside the pores which cannot be accessed at higher scan rates, probably due to the limited transfer of OH^- to such sites[21)] and some Ni sites fail to undergo redox processes at high potential sweep rates. Hence, the specific capacitance obtained at the slower scan rate is believed to be closer to that of the full utilization of the electro-active material.[22)]

Fig. 4 compares the cyclic voltammograms of Mn oxides deposited onto porous Ni (MnO_x/P-Ni) to the one deposited onto a flat Ni substrate (MnO_x/Ni) both recorded in 2 M NaOH electrolyte at 25°C with a potential scan rate of 20 mV s^{-1}. It is found that the CV enclosed area, which corresponds to charge storage capability, of MnO_x/P-Ni is much larger than that of MnO_x/Ni. The specific pseudo- capacitance of MnO_x/Ni calculated from Fig. 4 is 136 F g^{-1}. Interestingly, an exceptionally high capacitance of 1486 F g^{-1} has been obtained for Mn oxide dispersed on the porous Ni substrate (MnO_x/P-Ni). The high surface area of the conductive Ni substrate could expand the active sites for pseudocapacitive reaction and improve the utilization (or reactivity) of the Mn oxide. Moreover, the highly porous structure of the Ni pellet with the so-dispersed Mn oxide would enhance the access probability of electrolyte and therefore promote the ionic transportation within the electrode. Accordingly, the excellent electrochemical performance can be obtained. More importantly the MnO_x flakes are so

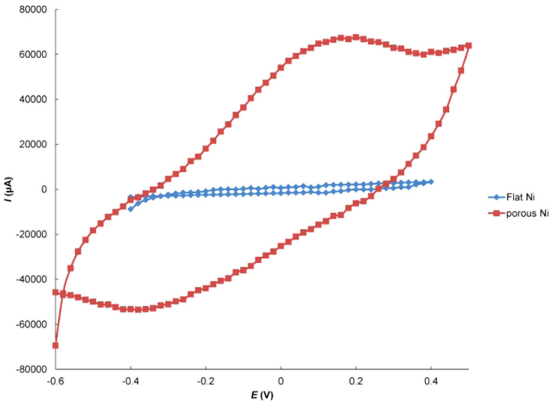

Fig. 4. CVs of the Mn oxide electrodes with the porous Ni substrate (curve a) and a flat Ni substrate (curve b) in 2 M NaOH electrolyte at 25°C at 20 mV s^{-1} scan rate.

thin that the entire material can indeed undergo charge transfer processes.

Fig. 4 also shows that the potential window of Mn oxide/P-Ni is somewhat broaden than Mn oxide/Ni being 1 V compared to 0.7 V.

Specific energy (E), specific power (P) and coulomb efficiency (η%) are calculated using following equations:

$$E = \frac{\Delta V \times I_d \times t_d}{W} \quad (4)$$

$$P = \frac{\Delta V \times I_d}{W} \quad (5)$$

$$\eta(\%) = \frac{T_d}{T_c} \times 100 \quad (6)$$

where ΔV, I_d and T_d are the discharge voltage variation, the discharge current, and discharge time, respectively. T_C is the charge time and (W) is the mass of Mn oxide film. The values of specific energy (E), specific power (P) and coulomb efficiency (η%) obtained from charge/ discharge curves are 212.1 Wh kg^{-1}, 5.1 kW kg^{-1}, and 98.6%, respectively.

The evaluation of supercapacitors for their specific power and specific energy has been of great interest because both high specific power and specific energy are desirable. The variation of specific power with specific energy for the as prepared materials is shown in Fig. 5. It is observed the specific Energy decreases upon increasing the current density from 5 mA to 8 mA while the specific power shows the opposite trend. The nano-porous structure of Mn oxide sample exhibits a good performance both in specific power and specific energy and it is a preferable electrode material for high-power supercapacitors.

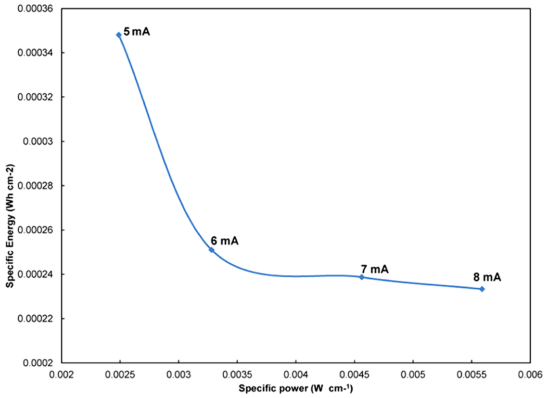

Fig. 5. Ragone plots showing variation of specific energy with specific power.

Voltammograms of MnO_x/P-Ni were obtained at different scan rates. The potential window in CVs was –0.6 V to 0.5 V and the scan rates were 5, 10, 20 and 50 mV/s. It was seen that the specific capacitance of MnO_x/P-Ni decreases with the increasing scan rate. It is well known that the pseudo-capacitive reaction of Mn oxide is a surface reaction, only the surface or a very thin surface layer of the oxide undergoes redox process in the course of a charge/discharge cycle.[29] Nano-porous structure facilitates protons' intercalation/deintercala- tion by increasing interficial area and providing easier access of the electrolyte to the Mn oxide sites.

The dependence of voltammetric charge, q, on $\nu^{-1/2}$ is shown in Fig. 6(a), and the inverse of the voltammetric charge, q^{-1}, is plotted as a function of the square root

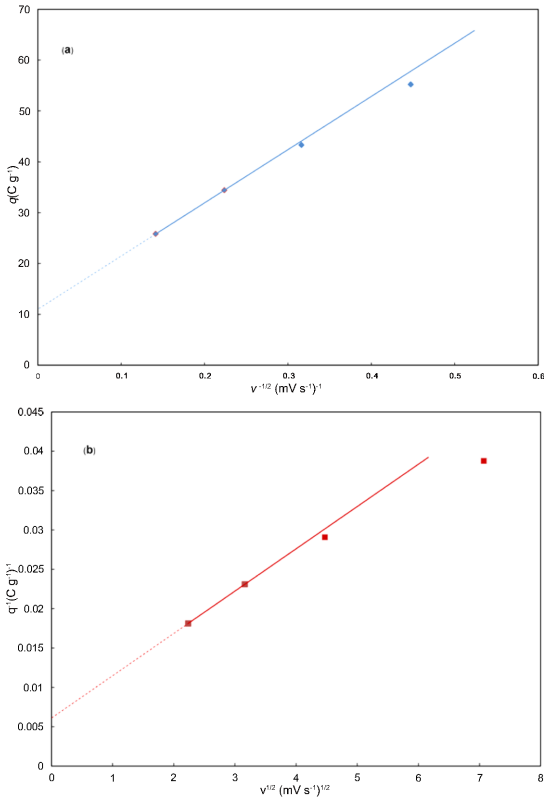

Fig. 6. Variation of the voltammetric charge density (q) with respect to scan rate (ν) (a) extrapolation of q to $\nu \rightarrow \infty$ from the q vs. $\nu^{-1/2}$ plot to get the outer charge and (b) extrapolation of q to $\nu \rightarrow 0$ from the q^{-1} vs. $\nu^{1/2}$ plot to get the total charge for MnO_x/P-Ni sample.

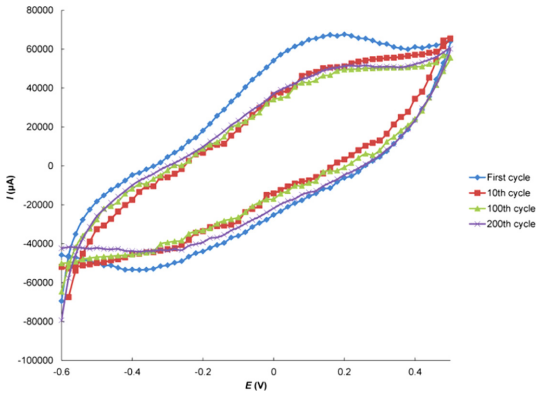

Fig. 7. CVs of Mn oxide o n porous Ni substrate in 2 M NaOH at 20 mV s^{-1} scan rate.

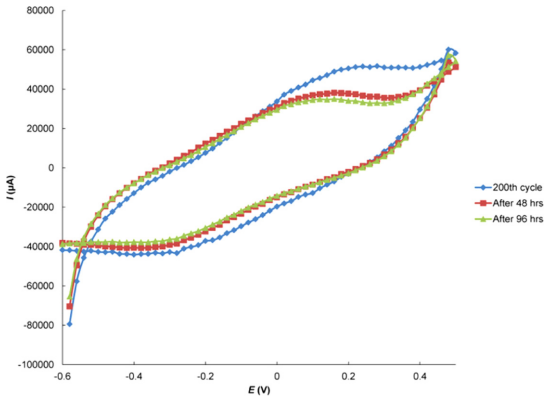

Fig. 8. CVs of MnO_x/P-Ni in 2 M NaOH at 20 mV s^{-1} scan rate.

of scan rate, $\nu^{1/2}$, as shown in Fig. 6(b). Voltammetric charge, q, increases with $\nu^{-1/2}$ (decreases with ν).The dependence of q on ν is usually explained by the existence of H^+ or OH^- in pores, cracks and grains boundaries.[29-31] The most of the protons at the surface of electrode are consumed at high scan rates therefore; this phenomenon limits the accessibility of protons to the inner surface of the electrode material at high scan rates. The electrochemical response then depends only on the outer active surface, which is easily accessed by protons. By the extrapolation of q to $\nu \rightarrow \infty$ from the q vs. $\nu^{-1/2}$ plot (Fig. 6(a)), the outer charge, q_o is obtained to be 11.00 C g^{-1}, which is related to the outer active surface. At low scan rates, protons have enough time to diffuse to the inner active surface. The extrapolation of q to $\nu \rightarrow 0$ in the q^{-1} vs. $\nu^{1/2}$ (Fig. 6(b)) gives the total charge; q_T, equal to 166.67 C g^{-1} which is related to the entire active material.

Stability of the Mn oxide deposited onto porous Ni electrode is also evaluated in the course of 200 CV cycles and the first, 10th, 100th and 200th cycles are presented in Fig. 7. Nearly 20% of capacitance decreased in first 10 cycles and it was retained during the next 200 charge/discharge cycles.

Stabilities of the prepared electrodes were examined both in the course and after 200th cycle. Cyclic voltammograms were recorded after two 48 h periods of keeping the electrodes dry and at room temperature. The results are presented in Fig. 8. While a 20% decay of the initial capacitance is observed, no further loss is witnessed signifying the stability of MnO_x/P-Ni system.

The charge/discharge behaviors of MnO_x/P-Ni at constant currents of ±8 mA are presented in Fig. 9. The discharge profile consists of two parts: a sharp potential drop due to the internal resistive components of materials is followed by the discharge of a capacitive component.

The ohmic drop is significantly smaller in comparison with other Mn oxides electrodes prepared by deposition on flat substrates.[5,6,25] This improvement in charge/ discharge behavior in porous-structured electrodes can be attributed to three major factors: (i) the high porosity increases OH transport, promoting ionic conduction within the electrode (ii) the largely dispersed Mn oxide shortens the electron travelling distance, within the material improving the electronic conduction, and (iii) the high contact area between the substrate and the electro-active material minimizes the interfacial resistance, facilitating charge transfer.[26]

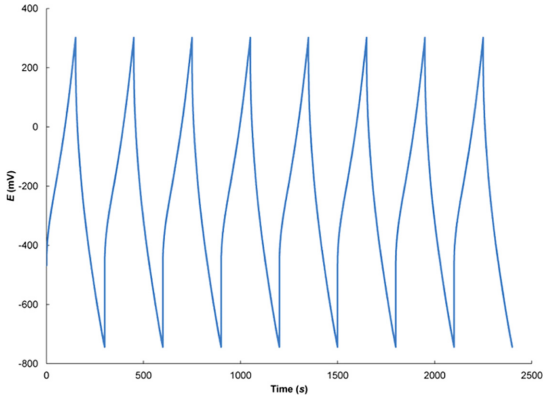

Fig. 9. The charge and discharge curve of Mn oxide on porous Ni in 2 M NaOH electrolyte. The charging current was 8 mA.

Fig. 9 presents the repeated cycles of charge-discharge in the time span of 2500 s. No shape and size changes were observed pointing to the reversibility as well as the stability of the system.

The specific capacitances of the electrodes are evaluated[23,24] using:

$$C = \frac{I \times t}{\Delta V \times m} \quad (7)$$

Where C is capacitance (F), I is current in the course of charge/ discharge processes, t the charge/discharge time, ΔV being the potential window and m is the mass of the electrodeposited materials which is 1.1×10^{-3} g. From the charge–discharge profile the specific capacitance is estimated to be 1515 F g^{-1}.

The surface area of MnO_x flakes can be calculated by the following equation:

$$S_{act} = \frac{Q}{Q_d} \quad (8)$$

Where S_{act} is electrochemical active surface area, Q (in C) the charge stored in MnO_x/P-Ni and Q_d (in C cm^{-2}) the charge stored on unit area of MnO_x/Ni. Q and Q_d were evaluated using CVs in Fig. 4. S_{act} was obtained to be 40.2 cm^2.

From the charge/discharge chronopotentiograms, Fig. 7, specific capacitance was derived to be 1515 F g^{-1}. Considering the theoretical capacitance of Mn-oxide[4] which is assumed to be 1380 F g^{-1}, it seems that not only the entire bulk of nano-flakes is involved in charge storage but also an additional 135 F g^{-1} (3.3 mF cm^{-2}) capacity exists that is in the range of adsorption capacitances and is probably due to the adsorption of OH^- on the high surface area (40.2 cm^2) of the assemblies of the flakes. This additional capacitance co-insides well with the values expected from adsorption. Capacitance as high as 2600 F g^{-1} has recently been reported[28] for nano-flakes (6 nm thick) of NiOOH in alkaline solutions where excess from theoretical value that corresponds to 325 F g^{-1} (0.6 mF cm^{-2}) has been attributed to double layer charging.

The retention of charge was further tested by studying the sample previously charged at 8 mA current and was kept in electrolyte for 600 s and was sequentially discharged at −8 mA, Fig. 10. As it is observed the stored charge has been retained after 600 s retention time and the discharge curve shows good similarity to the discharge process of the freshly charged electrodes.

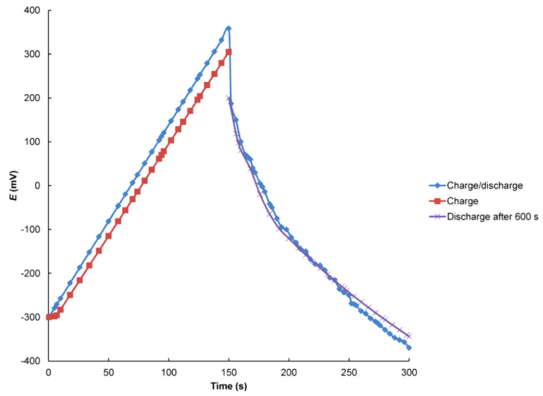

Fig. 10. The charge-discharge, charge and discharge curves of MnOx/P-Ni electrode in 2 M NaOH electrolyte. The charging current was 8 mA.

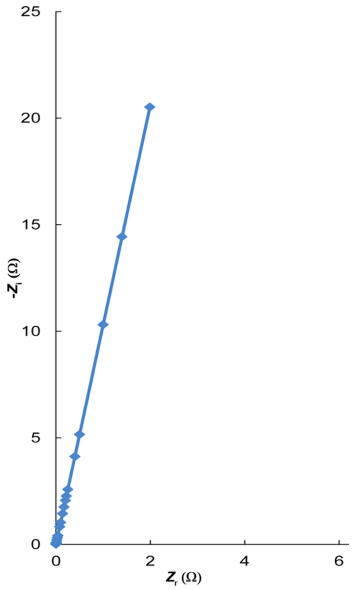

Fig. 11. The Nyquist plot for Mn oxide on porous Ni substrate at 0.1 V/SCE.

Fig. 11 presents the Nyquist plot for Mn oxide on porous Ni substrate recorded at 0.1 V/SCE where Z_r and Z_i are the real and imaginary parts of the impedance, respectively.

As it is seen MnO_x/P-Ni substrate exhibits almost ideal capacitive behavior. Fairly low real resistance of the system at the high frequency end of the spectrum is close to the calculated resistance of the electrolyte and points to the good conductivity (negligible resistance) of the electrode material. Using the imaginary part of

impedance, Z_i, at low frequency of 5×10^{-2} Hz the specific capacitance was derived to be 1411 F g^{-1}.

The obtained specific capacitance was calculated on the basis of assuming ideal capacitive behavior. By replacing the capacitance with a constant phase element (*CPE*) where $(j\omega)$ term is replaced by $(j\omega)^p$ and comparing with C_s obtained from charge/discharge study, power of (*CPE*), (*CPE*-P), has been found to be 0.99 ($0 < P < 1$) at 0.1 V that shows MnO_x/P-Ni behaves very close to an ideal capacitor.

4. Conclusion

On the basis of this work it is concluded that porous Ni pellets produced by leaching provides macro-pores where nano-flakes of Mn oxide can be electrodeposited onto and show huge capacitance. The entire bulk of Mn oxide undergoes charge/discharge and the capacitance exceeding the theoretical values points to the fact that its surface provides sites for OH^- adsorption and contributes additional capacitance of about 135 F g^{-1} (3.3 mF cm^{-2}).

Acknowledgment

The authors wish to express thanks to the office of vice chancellor of research of Sharif University of Technology for the financial support.

References

1. R. Kötz and M Carlen, *Electrochim. Acta*, **45**, 2483 (2000).
2. H. Y. Lee and J. B. Goodenough, *J. Solid State Chem.*, **144**, 220 (1999).
3. S. C. Pang, M. A. Anderson, and T. W. Chapman, *J. Electrochem. Soc.*, **147**, 444 (2000).
4. M. Toupin, T. Brousse and D. B'elanger, *Chem. Mater.*, **16,** 3184-319 (2004).
5. J. K. Chang, M. T. Lee and W. T. Tsai, *J. Power Sources*, **166**, 590 (2007).
6. H. Y. Lee, S. W. Kim and H. Y. Lee, *Electrochem. Solid State Lett.*, **4**, A19 (2001).
7. M. Toupin, T. Brousse and D. Bélanger, *Chem. Mater.*, **14**, 3946 (2002).
8. Y. U. Jeong and A. Manthiram, *J. Electrochem. Soc.*, **149**, A1419 (2002).
9. C. C. Hu and T. W. Tsou, *J. Power Sources*, **115**, 179 (2003).
10. H. Kim and B. N. Popov, *J. Electrochem. Soc.*, **150**, D56 (2003).
11. J. K. Chang and W. T. Tsai, *J. Electrochem. Soc.*, **150**, A1333 (2003).
12. V. Subramanian, H. Zhu, R. Vajtai, P. M. Ajayan and B. Wei, *J. Phys. Chem. B*, **109**, 20207 (2005).
13. W. C. West, N. V. Myung, J. F. Whitacre and B. V. Ratnakumar, *J. Power Sources*, **126**, 203 (2004).
14. X. Wang, X. Wang, W. Huang, P. J. Sebastian and S. Gamboa, *J. Power Sources*, **140**, 211 (2005).
15. C. L. Xu, S. J. Bao, L. B. Kong, H. Li and H. L. Li, *J. Solid State Chem.,* **179**, 1351 (2006).
16. Y. T. Wu and C. C. Hu, *J. Electrochem. Soc.*, **151**, A2060 (2004).
17. Y. K. Zhou, B. L. He, F. B. Zhang and H. L. Li, *J. Solid State Electrochem.*, **8**, 482 (2004).
18. E. Raymundo-Piñero, V. Khomenko, E. Frackowiak and F. Béguin, *J. Electrochem. Soc.*, **152**, A229 (2005).
19. C. Y. Lee, H. M. Tsai, H. J. Chuang, S. Y. Li, P. Lin and T. Y. Tseng, *J. Electrochem. Soc.*, **152**, A716 (2005).
20. L. Sun, C. L. Chien and P. C. Searson, *Chem. Mater.*, **16**, 3125 (2004).
21. K. H. Chang and C. C. Hu, *J. Electrochem. Soc.*, **151**, A958 (2004).
22. V. Gupta, T. Kusahara, H. Toyama, S. Gupta and N. Miura, *Electrochem. Commun.,* **9,** 2315 (2007).
23. F. Fusalba, R. Gouérec, D. Villers and D. Bélanger, *J. Electrochem. Soc.,* **148**, A1 (2001).
24. J. H. Park and O. O. Park, *J. Power Sources*, **111**, 185 (2002).
25. V. Subramanian, H. W. Zhu and B. Q. Wei, *Electrochem. Commun.*, **8**, 827 (2006).
26. C. M. Wu, C. Y. Fan, I. W. Sun, W. T. Tsai and J. K. Chang, *J. Power Sources*, **196**, 7828 (2011).
27. S. Chou, F. Y. Cheng and J. Chen, *J. Power Sources*, **162**, 727 (2006).
28. Z. Lu, Z. Chang, W. Zhu and X. Sun, *Chem. Commun.*, **47**, 9651 (2011).
29. Y. Zhang, J. Li, F. Kang, F. Gao and X. Wang, *Int J Hydrogen Energy*, **37**, 860 (2012).
30. C J. Xu, B. H. Li, H. D. Du, F. Y. Kang and Y. Q. Zeng, *J. Power Sources*, **180**, 664 (2008).
31. J. Yan, T. Wei, J. Cheng, Z. J. Fan and M. L. Zhang, *Mater. Res. Bull.*, **45**, 210 (2010).